Planetary and Space Science 106 (2015) 108–115

Contents lists available at ScienceDirect

Planetary and Space Science

journal homepage: www.elsevier.com/locate/pss

Pressure balance across the magnetopause: Global MHD results

J.Y. Lu [a], M. Wang [a,*], K. Kabin [b], J.S. Zhao [c], Z.-Q. Liu [d], M.X. Zhao [e], G. Li [a]

[a] Institute of Space Weather, School of Math & Statistics, Nanjing University of Information Science & Technology, Nanjing 210044, China
[b] Department of Physics, Royal Military College of Canada, Kingston, Ontario, Canada
[c] Purple Mountain Observatory, Chinese Academy of Sciences, 210008 Nanjing, China
[d] Center for Space Science and Applied Research, Chinese Academy of Sciences, Beijing 100080, China
[e] National Center for Space Weather, China Meteorological Administration, Beijing 100081, China

ARTICLE INFO

Article history:
Received 29 May 2014
Received in revised form
27 September 2014
Accepted 2 December 2014
Available online 10 December 2014

Keywords:
Pressure balance
Energy conversion
Magnetopause
Magnetohydrodynamic

ABSTRACT

The equilibrium magnetopause location on the dayside is determined by the balance of pressure forces. In this paper we use a physics-based global magnetohydrodynamic (MHD) to examine contributions of different terms to this balance. We calculate the total pressure, as well as thermal and magnetic pressures just inside and just outside the magnetopause. Our results show that (1) the total pressure just outside the magnetopause is enhanced with the increasing of B_Z in both northward and southward interplanetary magnetic field (IMF). For southward IMF the thermal pressure is dominant in the total pressure while the magnetic pressure is dominant for northward IMF when B_Z is not small ($B_Z > 5$ nT). For southward IMF larger solar wind dynamic pressure further enhances thermal pressure near the magnetopause while for northward IMF the dynamic pressure is more effectively converted to the magnetic pressure; (2) the thermal pressure just outside the magnetopause is significantly enhanced with the increasing southward IMF as compared to the northward IMF case. However, this enhanced thermal pressure is not the only reason for the well-known earthward displacement of the magnetopause under southward IMF conditions. The dayside magnetic reconnection for southward IMF dramatically decreases magnetic pressure just inside the magnetopause. The combination of these two factors explains the Earthward motion of the magnetopause for southward IMF.

1. Introduction

The magnetopause, one of the most important interfaces in the magnetosphere, separates solar wind from the area controlled by the geomagnetic field. Although terrestrial magnetopause is almost always observed in motion, on average pressure balance holds across the magnetopause [see, e.g., the discussion in Shue and Chao (2013)]. The classical pressure balance equation across the magnetopause can be written as (Schield, 1969)

$$kP_d = \frac{(fB_e)^2}{2\mu_0 R_c^6} + P_{th}^{in} \quad (1)$$

where $P_d = \rho_{sw} v_{sw}^2$ is the solar wind dynamic pressure (ρ_{sw} and v_{sw} are solar wind density and speed upstream of the bow shock), P_{th}^{in} is the thermal pressure just inside the magnetopause, B_e is the equatorial strength of the terrestrial dipole on the surface of the Earth, R_c is the magnetopause subsolar standoff distance measured in Earth radii (R_E), and μ_0 is the vacuum permeability. Factor k which appears in this equation describes the conversion of dynamic pressure of the solar wind upstream of the bow shock to total pressure at the stagnation point on the surface of the magnetopause. In gas-dynamic approximation assuming a normal shock $k=0.881$ for $\gamma=5/3$ (Schield, 1969). For plasma flow, this coefficient depends on the orientation and intensity of the magnetic field and was shown by Shue and Chao (2013) to be a significant contributor to the magnetopause erosion. Another factor, f is the ratio of the magnetic field just inside the magnetopause to that of a pure dipole at the same distance. It is often assumed that $f=2$ based on a simple analytical solution for a dipole confinement by an infinite plane. For Chapman–Ferraro problem it was computed to be $f=2.44$ (Beard, 1964). Change in f is usually considered to be the reason for smaller magnetopause standoff distances under southward IMF conditions as compared to the northward case. It is worth mentioning that Eq. (1) neglects dynamic pressure on either side of the magnetopause which is certainly justified near the stagnation point on the Sun–Earth line. Data analysis of Shue and Chao (2013) also demonstrated that the dynamic pressure is insignificant near the subsolar magnetopause.

To a first approximation, the location of the magnetopause is determined by the pressure balance between the solar wind and

* Corresponding author.
E-mail addresses: jylu@nuist.edu.cn (J.Y. Lu), mwang01@outlook.com (M. Wang), konstantin.kabin@rmc.ca (K. Kabin), js_zhao@pmo.ac.cn (J.S. Zhao), zqliu@spaceweather.ac.cn (Z.-Q. Liu), zhaomx@cma.gov.cn (M.X. Zhao), ligang@nuist.edu.cn (G. Li).

http://dx.doi.org/10.1016/j.pss.2014.12.003
0032-0633/

geomagnetic field. It is well known (Shue, 1998; Lu et al., 2010) that higher solar wind dynamic pressure pushes the magnetopause close to the Earth, while lower solar dynamic pressure lets the magnetopause to retreat further away from the Earth. Dynamic pressure of the solar wind clearly plays the dominant role in this pressure balance because of high Alfvénic and sonic Mach numbers in the free-streaming solar wind. However, the solar wind dynamic pressure is not the only factor controlling the magnetopause location. Orientation of the interplanetary magnetic field (IMF) also affects the magnetopause standoff distance. For comparable solar wind dynamic pressures, magnetopause is found closer to the Earth for southward direction of the IMF than for the northward, a phenomenon known as the "magnetopause erosion" (Maltsev and Lyatsky, 1975; Holzer and Slavin, 1978).

Magnetopause erosion is usually associated with magnetic reconnection occurring near the subsolar point which results in the decrease of the magnetic pressure just inside the magnetopause (Gosling et al., 1982; Aubry et al., 1971; Fairfield, 1971). Very recently, Shue and Chao (2013) used THEMIS data with smaller B_Z ($|B_Z| \le 4$ nT) to study observationally the role of enhanced thermal pressure in the pressure balance of the magnetopause. They, however, concluded that the earthward motion of the magnetopause for southward IMF is explained to a smaller extend by enhancement of the magnetosheath thermal pressure than by reduction of the magnetic pressure just inside the magnetopause. Thus, the results from Shue and Chao (2013) represent a significant modification of the generally accepted mechanism of the magnetopause erosion.

In this paper we use global MHD simulations of the terrestrial magnetosphere to investigate the pressure balance across the subsolar magnetopause. We also compute various contributions to pressure just inside and just outside the magnetopause. In agreement with previous results we find that thermal pressure just outside the magnetopause for southward IMF is enhanced compared with that for northward IMF. However, the enhanced thermal pressure is not the reason for the magnetopause earthward motion, because the total pressure just outside the magnetopause does not increase for southward IMF. Actually, our results show that the decreasing of the magnetic pressure just inside the magnetopause makes the main contribution to the decreasing of the subsolar standoff distance.

2. Simulation and methods

2.1. The simulation

Global MHD simulations allow immediate calculation of all the parameters appearing in Eq. (1) and, therefore a detailed analysis of the contributions from different terms. Using simulations, we can perform most of the analysis right on the Sun–Earth line, in contrast to observations which, because of the nature of spacecraft orbits, generally have to be projected to this line using some empirical model (Shue and Chao, 2013). In this work, the Space Weather Modeling Framework (SWMF) developed by University of Michigan is used to simulate the coupling between solar wind and magnetosphere (see the study by Tóth et al. (2005)). The SWMF is integrated by the numerical modules including the Solar Corona, Eruptive Event Generator, Inner Heliosphere, Solar Energetic Particles, Global Magnetosphere, Inner Magnetosphere, Ionosphere Electrodynamics, and Upper Atmosphere. The SWMF can provide a high-performance flexible framework for physics-based space weather simulations, as well as for various space physics applications. Especially, it has been used extensively to study various solar wind influences on the magnetosphere (e.g., Song and Russell, 1992; Kabin et al., 2004; Gombosi et al., 2000; Zhang, 2007; Tóth et al., 2007), and the validation of SWMF has been also discussed by many works (e.g., Welling and Ridley, 2010; Rae, 2010). Recently, we have also used the SWMF to do several works about the magnetopause. Lu et al. (2010, 2013a), and Liu et al. (2012) constructed and compared a new global magnetopause model from SWMF simulations with empirical models. Lu et al. (2013b) and Jing et al. (2014) used the SWMF to study the energy transfer across magnetopause for different solar wind conditions. These works all further demonstrated the effectiveness and reliability of SWMF.

In a typical simulation used in this work, the computational domain is defined by $-40R_E \le X \le 20R_E$ and $-40R_E \le Y, Z \le 40R_E$ in GSM coordinates, the inner boundary is a sphere with a radius of $2.5R_E$. The grid size inside $6.5R_E$ is $1/8R_E$; on the dayside, including the cusps and much of the magnetosheath it is $1/4R_E$, and in other areas it is $1/2R_E$. In our calculations, the solar wind dynamic pressure P_d is either 1 or 2 nPa. For $P_d = 1$ nPa, the plasma speed $V_X = -345.8$ km/s and $V_Y = V_Z = 0$ km/s, the plasma number density $n = 5$ cm^{-3}; for $P_d = 2$ nPa, the plasma speed $V_X = -450.0$ km/s and $V_Y = V_Z = 0$ km/s, the plasma number density $n = 6$ cm^{-3}. The values of IMF B_Z considered were $-20, -15, -10, -5, 0, 5, 10, 15$, and 20 nT, and $B_X = B_Y = 0$ nT. The dipole tilt angle is zero.

2.2. Identification of magnetopause subsolar standoff distance

It should be noted that there are several somewhat different definitions of the magnetopause, as discussed for example by Lu et al. (2010). Furthermore, the displacement of the stagnation point with respect to the X-line (Cassak and Shay, 2007, 2009) for asymmetric reconnection always leads to some internal structure of the magnetopause which therefore is not a mathematical surface. However, on the dayside the difference in the location of the magnetopause determined by alternative definitions is always small, so these variations are not important for the present work. Magnetopause in the simulations is identified using automated methods discussed at length by Lu et al. (2010); Liu et al. (2012); Lu et al. (2013a), Liu et al. (2012) and Lu et al. (2013a) and Lu et al. (2013b). In the subsolar region these methods are largely based on the maximum of the density gradient. The magnetopause identification and

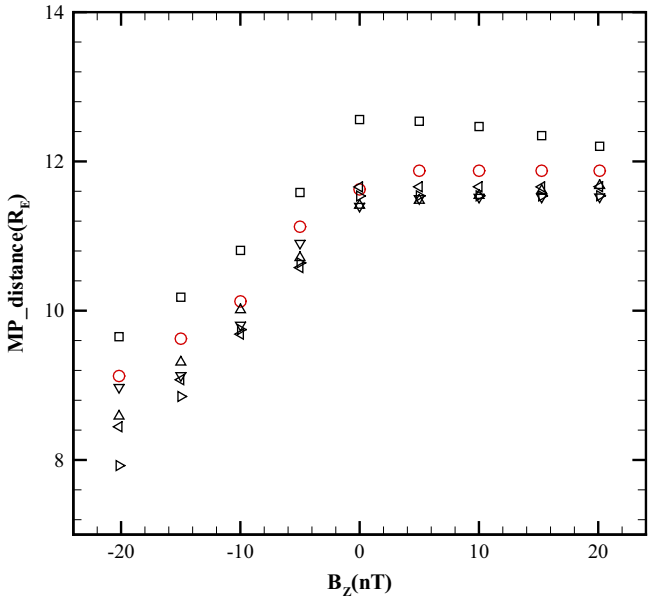

Fig. 1. The subsolar standoff distance as a function of the IMF B_Z for an MHD model and several empirical models. Red circles show our simulations; upward triangles (Shue et al., 1997); downward triangles (Shue, 1998); left triangles (Petrinec and Russell, 1996); right triangles (Chao et al., 2002); squares (Lin et al., 2010). The solar wind dynamic pressure was $P_d = 1$ nPa for all cases. (For interpretation of the references to color in this figure caption, the reader is referred to the web version of this article.)

validation of the resulting magnetopause model using available empirical models is also described in the references above.

Fig. 1 shows the validation of the subsolar standoff distance judged by the method of the maximum of plasma density gradient. The red circles stand for the subsolar standoff distance R_0 identified in our simulations. The black symbols represent the subsolar standoff distance calculated by the several frequently used magnetopause empirical models (Shue et al., 1997; Shue, 1998; Petrinec and Russell, 1996; Chao et al., 2002; Lin et al., 2010). The solar wind conditions used for this plot were $P_d = 1$ nPa, $B_Z = -20, -15, -10, -5, 0, 5, 10, 15, 20$ nT. Clearly, the subsolar standoff distances determined by the method of maximum density gradient in our simulations agree well with the results from empirical models. The difference of the subsolar standoff distances between our numerical results and empirical models for a fixed B_Z is usually within $0.5R_E$.

Fig. 1 also clearly shows the phenomena of the magnetopause erosion: for northward IMF the magnetopause location is essentially independent of the IMF intensity, but for southward IMF the magnetopause gets closer to the Earth when the IMF intensity increases. Note that the dynamic pressure is the same for all cases in Fig. 1, therefore this earthward displacement is associated with changes in the parameters k and f.

3. Numerical results

3.1. The pressure quantities just outside the magnetopause

In this section we discuss the pressure in the magnetosheath just outside the magnetopause. After determining the subsolar magnetopause standoff distance, we take the parameters just one grid point away from the subsolar magnetopause on the Sun–Earth line to calculate the pressure quantities just outside the magnetopause.

Fig. 2 shows the comparisons between the pressure quantities just outside the magnetopause for southward and northward IMFs for solar wind dynamic pressure $P_d = 1$ nPa (Fig. 2a) and 2 nPa (Fig. 2b). The pressure quantities, including thermal, magnetic, and total pressures, are plotted against the absolute value of B_Z. Solid and dashed curves represent variations for southward IMF and northward IMF, respectively. Different colors are used to show the variations in pressure just outside the magnetopause: blue for thermal pressure (P_{th}^{out}), red for magnetic pressure (P_b^{out}), and black for the total pressure ($P_t^{out} = P_{th}^{out} + P_b^{out}$).

From Fig. 2a we can see, when the absolute value of B_Z increases the thermal pressure is enhanced for southward IMF but decreased for northward IMF, consistent with the conclusions of Shue and Chao (2013). The magnetic pressure, however, is enhanced with the increasing of northward IMF but remains very low and almost independent of the IMF strength for southward IMF. The total pressure is enhanced with the increasing B_Z for both southward and northward IMF, and the increasing range of the total pressure for northward IMF is always larger than that for southward IMF under the same absolute value of B_Z. Fig. 2b is similar to Fig. 2a but corresponds to a larger solar wind dynamic pressure $P_d = 2$ nPa. Clearly, all the conclusions for $P_d = 1$ nPa still hold for this case as well.

Fig. 3 shows the dependence of the factor k on the interplanetary magnetic field. The factor k in our work is calculated by dividing the total pressure just outside the magnetopause by the solar wind dynamic pressure. The Z component of interplanetary magnetic field

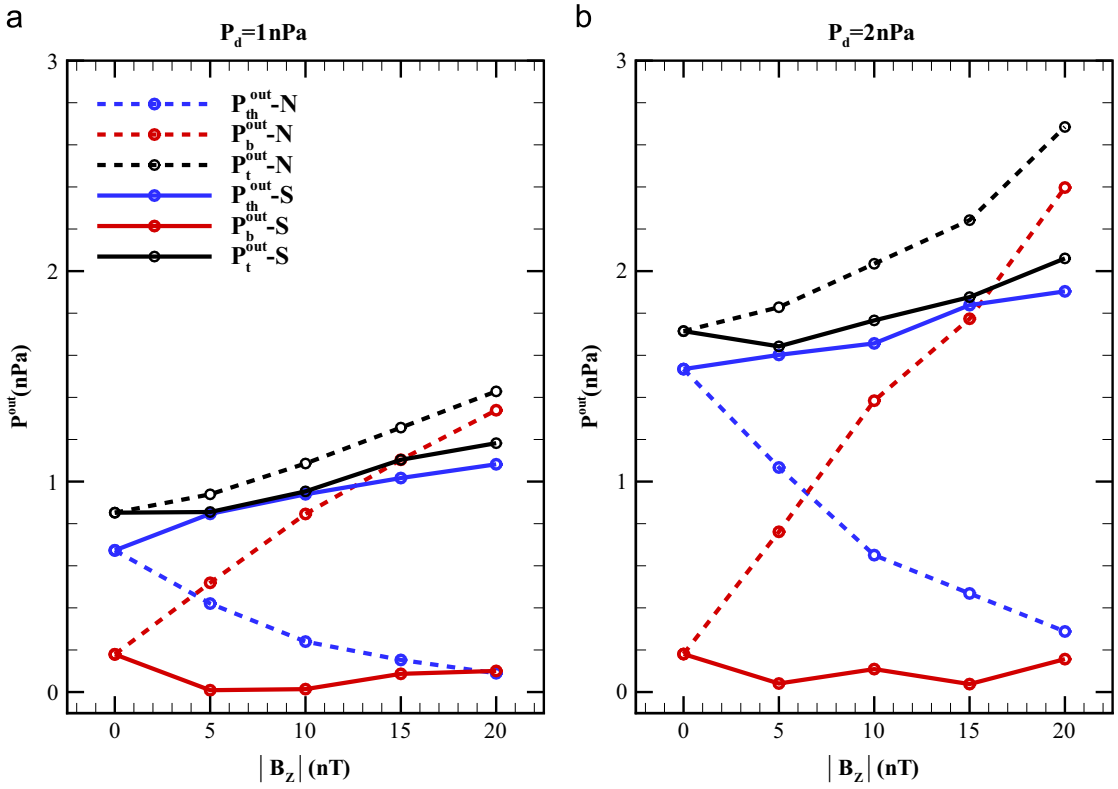

Fig. 2. The pressure quantities just outside the magnetopause for southward and northward IMF as a function of the absolute value of B_Z. Panel (a) is for $P_d = 1$ nPa and panel (b) for $P_d = 2$ nPa. Solid and dashed curves represent variations for southward IMF and northward IMF, respectively. Different colors are used to show the variations in pressure just outside the magnetopause: blue for thermal pressure (P_{th}^{out}), red for magnetic pressure (P_b^{out}), and black for the total pressure ($P_t^{out} = P_{th}^{out} + P_b^{out}$). (For interpretation of the references to color in this figure caption, the reader is referred to the web version of this article.)

$B_Z = -20, -15, -10, -5, 0, 5, 10, 15, 20$ nT, respectively. Panels (a) and (b) correspond to $P_d = 1$ nPa and $P_d = 2$ nPa, respectively.

From Fig. 3 we can see, k increases with the increasing of B_Z for both northward and southward IMF. However, for the same absolute value of B_Z, the value of k for northward IMF is larger than that for southward. When the solar wind dynamic pressure P_d is equal to 2 nPa the relationships between k and IMF remain qualitatively similar, however for the same value of B_Z, the stronger solar wind dynamic pressure results in a somewhat smaller value of k. This effect is particularly obvious for northward IMF.

3.2. The pressure quantities just inside the magnetopause

We take the points just one grid point closer to the Earth from the subsolar magnetopause on the Sun–Earth line to calculate the pressure quantities just inside the magnetopause. Fig. 4 shows the comparisons between the pressure quantities just inside the magnetopause for southward and northward IMF. The pressure quantities, including thermal, magnetic, and total pressures, are plotted against the absolute value of B_Z for the lower level of $P_d = 1$ nPa(a) and the higher level of $P_d = 2$ nPa(b). Solid and dashed curves are for

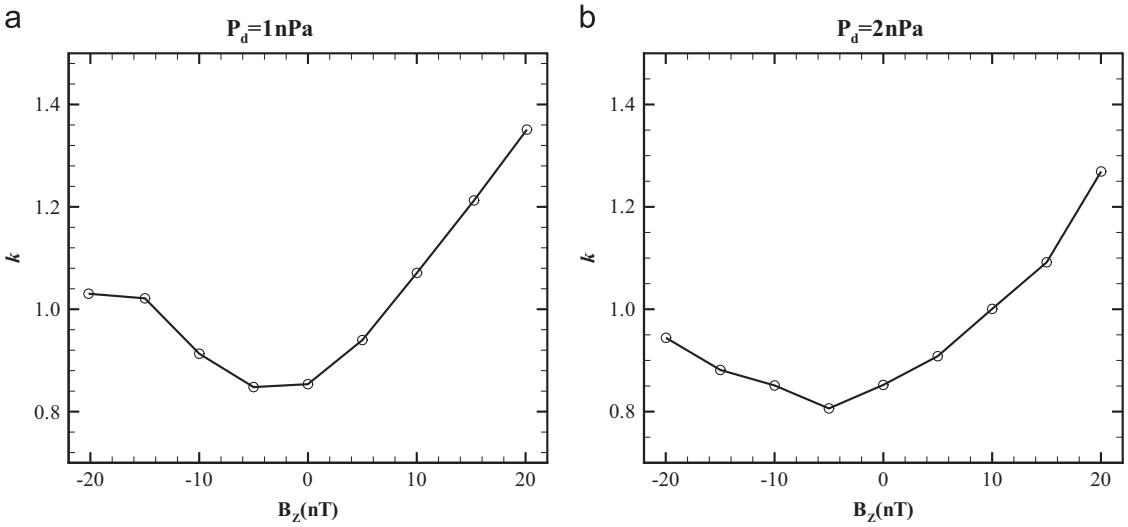

Fig. 3. Dependence of the factor k on the interplanetary magnetic field. (a) is for $P_d = 1$ nPa and (b) is for $P_d = 2$ nPa.

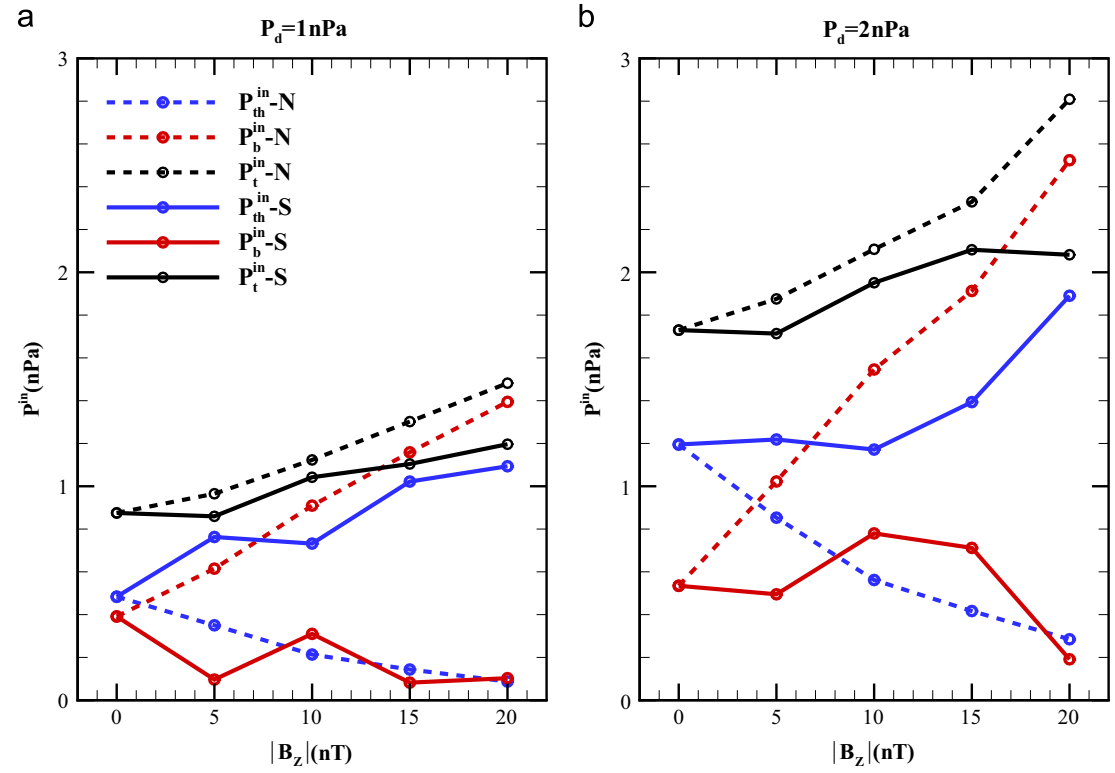

Fig. 4. The pressure quantities just inside the magnetopause for southward and northward IMF as functions of the absolute value of B_Z. (a) is for $P_d = 1$ nPa and (b) is for $P_d = 2$ nPa. Solid and dashed curves represent variations for southward IMF and northward IMF, respectively. Different colors are used to show the variations in pressure just inside the magnetopause: blue for thermal pressure (P_{th}^{in}), red for magnetic pressure (P_b^{in}), and black for the total pressure ($P_t^{in} = P_{th}^{in} + P_b^{in}$). (For interpretation of the references to color in this figure caption, the reader is referred to the web version of this article.)

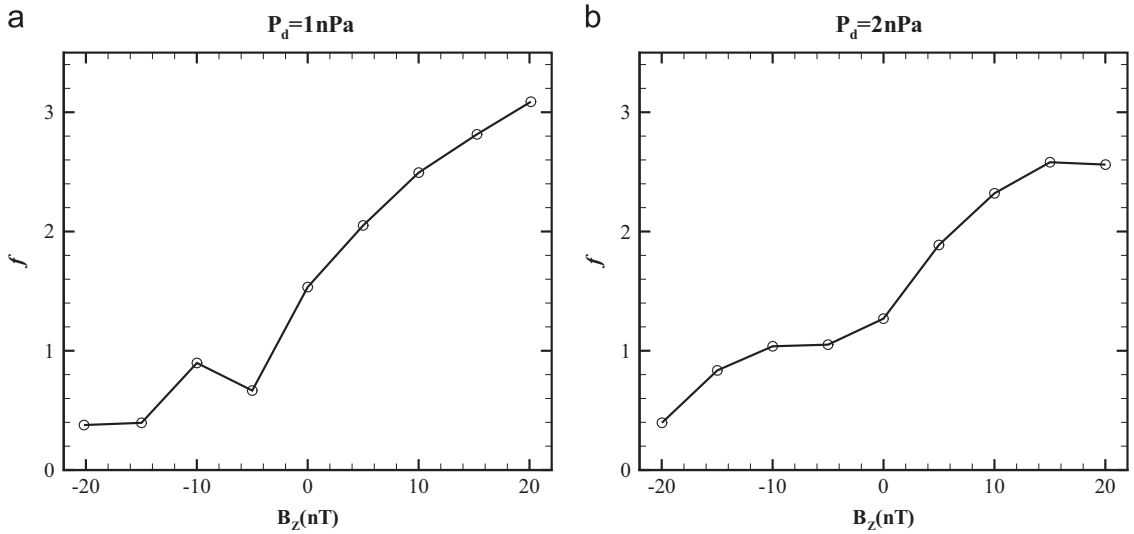

Fig. 5. Dependence of the factor f on the interplanetary magnetic field. The factor f is the ratio of the magnetic field just inside the magnetopause to that of a pure dipole at the same distance. (a) is for $P_d = 1$ nPa and (b) is for $P_d = 2$ nPa.

southward IMF and northward IMF, respectively. Blue color is used for thermal pressure (P_{th}^{in}), red for magnetic pressure (P_b^{in}), and black for the total pressure ($P_t^{in} = P_{th}^{in} + P_b^{in}$).

From Fig. 4 we can see, the total pressure just inside the magnetopause is enhanced with the increasing of B_Z for both northward and southward IMF. For southward IMF the thermal pressure is the dominant component of the total pressure and the magnetic pressure is dominant for northward IMF. However, for southward IMF, the magnetic pressure just inside the magnetopause for higher solar wind dynamic pressure is more than that for lower solar wind dynamic pressure.

Next, we examine the magnetic field compression ratio f just inside the magnetopause, shown in Fig. 5 as a function of the IMF strength. The factor f is defined as a ratio of the magnetic field just inside the magnetopause to the dipolar magnetic field at the same location if there were no solar wind. Panels (a) and (b) of Fig. 5 correspond to $P_d = 1$ nPa and $P_d = 2$ nPa, respectively. From Fig. 5 we can see, the factor f increases with the IMF and is substantially higher for positive (northward) than for negative (southward) IMF. This behavior remains qualitatively the same for the solar wind dynamic pressure P_d of either 1 or 2 nPa. We note that, for large northward IMF parameter f exceeds 2.44 which is computed for Chapman–Ferraro currents. In contrast, for southward IMF f approaches zero, consistent with the dayside reconnection point on the magnetopause.

4. Discussion

4.1. Pressure conversion

Why the influences of the northward and southward IMF on the pressure balance across the magnetopause are different? With this question, we first discuss the variation of the pressure quantities including the dynamic pressure, the thermal pressure, and the magnetic pressure along the Sun–Earth line for northward and southward IMF conditions. In Fig. 6, the black, blue, and red lines represent the dynamic pressure, the thermal pressure, and the magnetic pressure on the Sun–Earth line, respectively. The green dotted lines show for the magnetopause standoff distance determined in our work. The two panes of Fig. 6 correspond to (a) northward IMF of $B_Z = 10$ nPa and (b) southward $B_Z = -10$ nPa. The small points stand for the grid points in the simulation data. The upstream solar wind dynamic pressure P_d is 1 nPa in either case.

From Fig. 6 we can see that, when the solar wind plasma flows across the bow shock, the dynamic pressure gradually decreases until almost zero near the magnetopause for both southward and northward IMFs. Dynamic pressure remains very small inside the magnetopause as well. It, therefore, can be safely excluded from the analysis of the magnetopause location, as it was done in previous studies (Schield, 1969; Shue and Chao, 2013). For northward IMF, the magnetic pressure increases rapidly towards the Earth and is clearly the dominant term in the vicinity of the magnetopause. The character of the magnetic pressure increase does not change across the magnetopause. Along the Sun–Earth line, the thermal pressure reaches its peak in the magnetosheath, then decreases to its minimum after across the magnetopause, very slowly at first and then rather rapidly near the magnetopause. For southward IMF (Fig. 6b), the behavior of thermal and magnetic pressure terms is radically different. Magnetic pressure drops to nearly zero near the magnetopause, which is not surprising since this is where magnetic reconnection occurs. Thermal pressure jumps across the bow shock and then slowly decreases through the magnetosheath towards the Earth in a manner similar to the northward IMF case. However, close to the magnetopause the thermal pressure increases very rapidly and substantially as a result of energy conversion in the magnetic reconnection and becomes by far the dominant term in the pressure balance equation. The thermal pressure peak corresponds very well to the magnetopause location determined by the density gradient method. It should be noted that although the magnetopause location (the green dotted lines in Fig. 6) is determined from the maximum of the solar wind density gradient, it corresponds very well to the point where plasma dynamic pressure decreases to nearly zero and remains very low inside the magnetopause. This holds for both northward and southward IMF cases. The magnetopause location is also nearly 2 R_E closer to the Earth for southward IMF than for northward IMF.

The pressure conversions along the Sun–Earth line for the northward and southward IMF are different, we believe that the reason for this phenomenon is the magnetopause erosion as described by the early works of Maltsev and Lyatsky (1975) and Holzer and Slavin (1978). As we all know, when the IMF points northward which is the same orientation as the Earth's dipole magnetic field at the subsolar point, the magnetic reconnection is

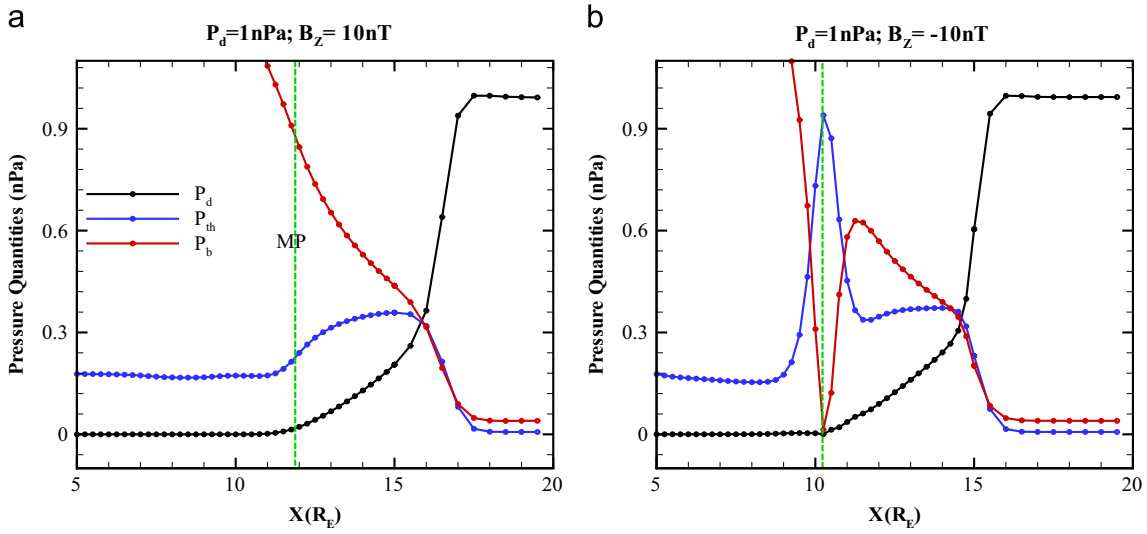

Fig. 6. The pressure dependence on distance along the subsolar line for northward (left panel) and southward (right panel) IMF. The black, blue and red lines represent the dynamic pressure, the thermal pressure, and the magnetic pressure respectively. The green dotted lines stand for the subsolar magnetopause locations in our simulations. The small points stand for the grid points in the simulation data. The solar wind dynamic pressure is 1 nPa in both cases. (For interpretation of the references to color in this figure caption, the reader is referred to the web version of this article.)

difficult to happen. So that the IMF lines can accumulate outside the subsolar magnetopause, the magnetic pressure caused by IMF just outside the magnetopause is increased by the increasing B_Z, and magnetic pressure near the subsolar magnetopause plays a dominant role which clearly exceeds all other pressure terms for northward IMF. For the southward IMF the magnetic reconnection is occurred at the subsolar magnetopause, as the x and y components of the IMF is equal to zero in our simulations, the magnetic field at the subsolar magnetopause is very small and the magnetic pressure is close to zero, too. As a result, for the southward IMF the upstream dynamic pressure mainly converts to thermal pressure outside the magnetopause, that is, it is the thermal pressure that is dominant. Of course, the above are the results when the B_Z is not small. For small B_Z, thermal pressure is always the dominant term. However, from Fig. 2 we can also get that for B_Z exceeding about 5.0 nT the magnetic pressure becomes larger than the thermal pressure. This is a new result which modifies the classical consideration of the pressure balance across the magnetopause. It should be noted, however, that currently there is no observational verification for this conclusion since the dataset in Shue and Chao (2013) was limited by $|B_Z| \leq 4$ nT. Periods of consistent high northward IMF are quite rare.

After understanding the mechanism of the pressure conversion for the different IMF orientations, we can explain the numerical results in Section 3 about the pressure balance across the subsolar magnetopause. As we mentioned above that the IMF lines cannot accumulate outside the magnetopause for southward IMF because of the magnetic reconnection. As a result, the magnetic pressure just outside the magnetopause remain almost independent of the magnitude of B_Z for southward IMF, and clearly increases with increasing northward B_Z. For a constant upstream dynamic pressure, so that the thermal pressure just outside the magnetopause decreases with the increasing northward B_Z and increases with the increasing southward B_Z. The increasing northward B_Z directly accumulates to the magnetic pressure outside the subsolar magnetopause; for the increasing southward B_Z, the magnetic pressure which should be increased by B_Z converts to the thermal pressure outside the subsolar magnetopause. Therefore, the total pressure just outside the magnetopause is enhanced by the increasing B_Z both of the southward and northward. However, because of the wastage when the magnetic pressure converts to the thermal pressure for southward B_Z, the total pressure just outside the magnetopause for northward IMF is actually larger than that for southward IMF for the same value of $|B_Z|$. As the factor k is the ratio of the total pressure just outside the magnetopause to the upstream dynamic pressure, for a constant upstream dynamic pressure, k is increased with the increasing B_Z both of the southward and northward, Moreover, for the same value of $|B_Z|$ the k for southward IMF is smaller than that for northward IMF. It should be noted that, because of the accumulation of the magnetic or thermal pressure just outside the subsolar magnetopause by the increasing $|B_Z|$, the total pressure just outside the subsolar magnetopause may become larger than the upstream dynamic pressure. As a result, the ratio k in our simulation might be greater than 1, especially for the larger $|B_Z|$.

If the magnetopause is in pressure balance, change in the outside pressure needs to be balanced by the corresponding change in the inside pressure. So that, the influences of the IMF on the pressure quantities just inside the magnetopause are very similar to that outside the magnetopause. Except that, for southward IMF, the magnetic pressure just inside the magnetopause for higher solar wind dynamic pressure is more than that for lower solar wind dynamic pressure. This is probably associated with the thickness of the reconnection layer in the simulation. We also would like to point out that for northward IMF the magnetopause standoff distance is virtually independent of the IMF intensity (Shue et al., 1997; Lu et al., 2010). In this case the total pressure just outside the magnetopause, which increases with increasing IMF intensity, is balanced by the corresponding increase in the f factor just inside the magnetopause. For southward IMF, the subsolar standoff distance decreases with the increasing B_Z. As the magnetic field near the magnetopause is always near zero for southward IMF, while the dipolar magnetic field increases toward the Earth. As a result, the factor f decreases substantially for the increasing southward B_Z.

4.2. Magnetopause motion

Solar wind dynamic pressure (P_d) and the Z component of interplanetary magnetic field (B_Z) are the two main contributing parameters to the subsolar standoff distance, R_0, of the magnetopause. A larger solar wind dynamic pressure imposes more total pressure on the magnetopause, the subsolar standoff distance is decreased. In this work, we use $P_d = 1$ nPa($V_X = -345.8$ km/s, $n = 5$ cm^{-3}) for the

smaller dynamic pressure, and $P_d = 2$ nPa($V_X = -450.0$ km/s, $n = 6\ \mathrm{cm}^{-3}$) for the larger dynamic pressure. We can find that the relationships between the pressure quantities (including the thermal pressure, magnetic pressure and total pressure) and the IMFs are generally the same for both smaller and larger P_d, as well as the factors k and f. Moreover, from the numerical results in Section 3 we can also find that the factor f for a smaller P_d is very similar to that for a larger P_d under the same IMFs. However, the factor k for a smaller P_d is larger than that for a larger P_d under the same IMFs. The reason for this phenomenon is as follows: according to the theoretical derivation of the factor k by Spreiter et al. (1966), k decreases with the increasing upstream Mach number. The upstream Mach number is increased when the P_d increases from 1 nPa to 2 nPa with the increasing solar wind speed in our simulations, as a result, the factor k decreases with the increasing P_d (Note: this increment of P_d need come from the contribution of the solar wind speed). Nonetheless, the total pressure outside the magnetopause is still increased by the increasing P_d. So that, the magnetopause subsolar standoff distance is decreased with the increasing P_d.

Empirical magnetopause models (Shue et al., 1997; Shue, 1998; Petrinec and Russell, 1996; Chao et al., 2002; Lin et al., 2010) and our results all show that the subsolar standoff distance keeps almost unchanged for varying northward B_Z, and is decreased with the increasing southward B_Z. So the subsolar standoff distance is decreased when the IMF turns from northward to southward. Early theories of the phenomenon (Maltsev and Lyatsky, 1975; Holzer and Slavin, 1978) explained it in terms of the field-aligned currents, created by magnetic reconnection (Sonnerup et al., 1981) for southward IMF which reduce the magnetic pressure just inside the magnetopause. Shue and Chao (2013)'s results from observation show that the magnetopause earthward movement to its real position can not be explained only by the reduced magnetic pressure just inside the magnetopause, but an enhancement of the whole pressure just outside the magnetopause is needed. They further demonstrated that the most important part to the whole pressure enhancement comes from the enhanced thermal pressure.

The subsolar standoff distance decreases when the factor k increases when the P_d and the total pressure just inside the magnetopause are not changed. The value of the factor k depends upon the properties of the solar wind plasma (Spreiter et al., 1966), however this fact was typically not considered in discussions of the magnetopause standoff distance which focused instead on the geomagnetic field reduction by reconnection. Recent observations, though, demonstrate that the IMF orientation can modify k value (Jelínek et al., 2010; Suvorova et al., 2010; Shue and Chao, 2013). This change in the value of k can also shift the magnetopause location.

Our numerical results show that the factor k increases with the increasing B_Z not only for southward IMF but also for northward IMF. In fact, for the same absolute value of B_Z the factor k for northward IMF is larger than that for southward. Earthward motion of the magnetopause for increasingly strong northward IMF does not occur, however, because of the corresponding increase in the factor f, which describes the magnetic pressure inside the magnetosphere. Thus, the factor k itself may not be the only reason of the subsolar standoff distance decreasing when the IMF turns form northward to southward. However, for southward IMF the enhanced k occurs together with decrease in f and the combination of these two factors is responsible for the earthward motion of the magnetopause.

Our numerical result also shows that, for northward IMF, with the increasing of B_Z the enhanced magnetic pressure causes the increasing of the total pressure just outside the magnetopause, and the factor k increases. From Eq. (1) we know, the subsolar standoff distance decreases when the factor k increases. On the other hand, the factor f increases with the increasing B_Z, the increasing magnetic pressure just inside the magnetopause with the increasing B_Z causes the sunward movement of the magnetopause. The cancelation of these two factors causes almost no change in the subsolar standoff distance for increasing northward B_Z.

For southward IMF, with the increasing of B_Z the enhanced thermal pressure causes the increasing of the total pressure just outside the magnetopause, and the factor k increases, however, the factor f decreases with the increasing B_Z which indicate that just inside the magnetopause the increasing scale of the compressed magnetic pressure is less than the increasing scale of the Earth's dipolar magnetic pressure. The combined effect of the two factors is that the subsolar standoff distance decreases for increasing southward B_Z. Therefore, for southward IMF the increasing of the thermal pressure just outside the magnetopause caused by the increasing B_Z is an important reason of the subsolar standoff distance decreasing for increasing B_Z. Under the same absolute value of B_Z, because the total pressure just outside the magnetopause for southward IMF is less than that for northward, the major reason of the subsolar standoff distance decreasing when the IMF turns from northward to southward is the relatively decreasing of the magnetic pressure just inside the magnetopause.

The thermal pressure enhancement in the southward IMF is related to the magnetic field reconnection. Shue and Chao (2013) pointed out, on the one hand, magnetic reconnection that occurs during southward IMF can convert magnetic energy to kinetic energy and thermal energy; on the other hand, the magnetic reconnection can generate a blunter magnetopause, which makes the shocked solar wind more difficult to flow around the magnetopause. As a result, it provides the secondary effect on the enhanced thermal pressure of the magnetosheath. From our result, we conclude that for northward IMF the magnetic fields just outside the magnetopause can accumulate with increasing B_Z, while during southward IMF the loss of the magnetic fluxes due to the magnetic reconnection makes the magnetic field hardly accumulate, thus thermal pressure just outside the magnetopause becomes dominate.

5. Conclusions

We employ the global MHD code, Space Weather Modeling Framework (SWMF), to simulate the interaction between solar wind and magnetosphere for both southward and northward IMF under the solar wind dynamic pressure P_d is equal to 1 and 2 nPa. Comparisons with the empirical magnetopause models ensure that the maximum gradient of solar wind plasma density can be used very well to determine the subsolar standoff distance. We calculate the total pressures including the magnetic pressure and thermal pressure just outside and inside the magnetopause, as well as the commonly used factors k and f. Our study leads to the following conclusions:

(1) The total pressure just outside the magnetopause converted by solar wind dynamic pressure is enhanced with the increasing of B_Z for both northward and southward IMF. For southward IMF and modest northward IMF ($B_Z < 5$ nT) the thermal pressure is dominant in the total pressure, which is agreement with the recent observation conclusion. However, at least in our idealized simulations of this paper, the magnetic pressure becomes important and dominant for larger values of northward IMF B_Z. The important role of thermal pressure enhancement holds only for southward and small northward B_Z. In contrast, for large northward B_Z the enhanced magnetic pressure (not the thermal pressure) is the major contributor to the overall pressure enhancement. It should also be mentioned that currently there is no observational verification for

this conclusion since periods of consistent high northward IMF are quite rare.

(2) The factor k is enhanced with the increasing of B_Z for both northward and southward IMF. Under the same absolute value of B_Z the factor k for northward IMF is actually larger than that for southward IMF. The factor f increases with the increasing $|B_Z|$ for northward IMF, but decreases for southward IMF.

(3) For southward IMF the increasing of the thermal pressure just outside the magnetopause caused by the increasing B_Z is an important reason of the decreasing of the subsolar standoff distance for increasing B_Z. However, the thermal pressure does not play a crucial role in the earthward displacement of the Earth's magnetopause for southward IMF as opposed to the northward IMF. This effect is further enhanced by the decreasing of the magnetic pressure just inside the magnetopause which was the main focus of the earlier theories (Maltsev and Lyatsky, 1975; Holzer and Slavin, 1978).

Acknowledgements

The authors would like to thank Dr. J.-H. Shue for very helpful discussion and suggestions. This work was partially supported by the National Basic Research Program of China (No. 2012CB825606), the National Natural Science Foundation of China (Grant No. 41031063), the China Meteorological Administration (the CMA Grant No. GYHY201106011), the NUIST Talent Foundation and the China Public Science and Technology Research Funds Projects of Ocean (No. 201005017). Simulation results were obtained using BATS-R-US, developed by the Center for Space Environment Modeling at the University of Michigan.

References

Aubry, M.P., Kivelson, M.G., Russell, C.T., 1971. Motion and tructure of the magnetopause. J. Geophys. Res 76 (7), 1673–1696. http://dx.doi.org/10.1029/JA076i007p01673.

Beard, D.B., 1964. The solar wind geomagnetic field boundary. Rev. Geophys. 2 (335), 1964.

Cassak, P.A., Shay, M.A., 2007. Scaling of asymmetric magnetic reconnection: general theory and collisional simulations. Phys. Plasmas 14, 102114 http://dx.doi.org/10.1063/1.2795630.

Cassak, P.A., Shay, M.A., 2009. Structure of the dissipation region in fluid simulations of asymmetric magnetic reconnection. Phys. Plasmas 16, 055704 http://dx.doi.org/10.1063/1.3086867.

Chao, J.K., Wu, D.J., Lin, C.-H., Yang, Y.H., Wang, X.Y., Kessel, M., Chen, S.H., Lepping, R.P., 2002. Models for the size and shape of the Earth's magnetopause and bow shock, in space weather study using multipoint techniques, in: L. -H. Lyu (Ed.), COSPAR Colloq. Ser., vol. 12, Pergamon, Oxford, pp. 127–134.

Fairfield, D.H., 1971. Average and unusual locations of the Earth's magnetopause and bow shock. J. Geophys. Res. 76 (28), 6700–6716. http://dx.doi.org/10.1029/JA076i028p06700.

Gombosi, T.I., DeZeeuw, D.L., Groth, C.P.T., Powell, K.G., 2000. Magnetospheric configuration for Parker-spiral IMF conditions: Results of a 3D AMR MHD simulation. Advances in Space Research 26 (1), 139–149.

Gosling, J.T., Asbridge, J.R., Bame, S.J., Feldman, W.C., Paschmann, G., Sckopke, N., Russell, C.T., 1982. Evidence for quasi-stationary reconnection at the dayside magnetopause. J. Geophys. Res. 87 (A4), 2147–2158. http://dx.doi.org/10.1029/JA087iA04p02147.

Holzer, R.E., Slavin, J.A., 1978. Magnetic flux transfer associated with expansions and contractions of the dayside magnetosphere. J. Geophys. Res. 83 (A8), 3831–3839. http://dx.doi.org/10.1029/JA083iA08p03831.

Jelínek, K., Němeček, Z., Šáfranková, J., Shue, J.-H., Suvorova, A.V., Sibeck, D.G., 2010. Thin magnetosheath as a consequence of the magnetopause deformation: THEMIS observations. J. Geophys. Res. 115, A10203. http://dx.doi.org/10.1029/2010JA015345.

Jing, H., Lu, J.Y., Kabin, K., Zhao, J.S., Liu, Z.-Q., Yang, Y.F., Zhao, M.X., Wang, M., 2014. MHD simulation of energy transfer across magnetopause during sudden changes of the IMF orientation. Planet. Space Sci. doi: http://dx.doi.org/10.1016/j.pss.2014.04.001.

Kabin, K., Rankin, R., Rostoker, G., Marchand, R., Rae, I.J., Ridley, A.J., Gombosi, T.I., Clauer, C.R., De Zeeuw, D.L., 2004. Open-closed field line boundary position: a parametric study using an MHD model. J. Geophys. Res. 109, A05222. http://dx.doi.org/10.1029/2003JA010168.

Lin, R.L., Zhang, X.X., Liu, S.Q., Wang, Y.L., Gong, J.C., 2010. A three-dimensional asymmetric magnetopause model. J. Geophys. Res. 115, A04207. http://dx.doi.org/10.1029/2009JA014235.

Liu, Z.-Q., Lu, J.Y., Kabin, K., Yang, Y.F., Zhao, M.X., Cao, X., 2012. Dipole tilt control of the magnetopause for southward IMF from global magnetohydrodynamic simulations. J. Geophys. Res. 117, A07207. http://dx.doi.org/10.1029/2011JA017441.

Lu, J.Y., Liu, Z.-Q., Kibin, K., Zhao, M.X., Liu, D.D., Zhou, Q., Xiao, Y., 2010. Three dimensional shape of the magnetopause: global MHD results. J. Geophys. Res. 116, A09237. http://dx.doi.org/10.1029/2010JA016418.

Lu, J.Y., Liu, Z.-Q., Kabin, K., Jing, H., Zhao, M.X.,2013a. The IMF dependence of the magnetopause. J. Geophys. Res. doi: http://dx.doi.org/10.1029/2013JA018672.

Lu, J.Y., Jing, H., Liu, Z.-Q., Kabin, K., Jiang, Y., 2013b. Energy transfer across the magnetopause for northward and southward interplanetary magnetic fields. J. Geophys. Res., doi: http://dx.doi.org/10.1029/2012JA018336.

Maltsev, Y.P., Lyatsky, W.B., 1975. Field-aligned currents and erosion of the dayside magnetosphere. Planet. Space Sci. 23 (9), 1257–1260. http://dx.doi.org/10.1016/0032-0633(75)90149.

Petrinec, S.M., Russell, C.T., 1996. Near-Earth magnetotail shape and size as determined from the magnetopause flaring angle. J. Geophys. Res. 101 (A1), 137–152.

Rae, I.J., et al., 2010. Comparison of the open-closed separatrix in a global magnetospheric simulation with observations: the role of the ring current. J. Geophys. Res. 115, A08216. http://dx.doi.org/10.1029/2009JA015068.

Schield, M.A., 1969. Pressure balance between solar wind and magnetosphere. J. Geophys. Res. 74 (5), 1275–1286. http://dx.doi.org/10.1029/JA074i005p01275.

Shue, J.-H., Chao, J.K., Fu, H.C., Russell, C.T., Song, P., Khurana, K.K., Singer, H.J., 1997. A new functional form to study the solar wind control of the magnetopause size and shape. J. Geophys. Res. 102 (A5), 9497–9511. http://dx.doi.org/10.1029/97JA00196.

Shue, J.-H., et al., 1998. Magnetopause location under extreme solar wind conditions. J. Geophys. Res. 103 (A8), 17691–17700. http://dx.doi.org/10.1029/98JA01103.

Shue, J.-H., Chao, J.-K., 2013. The role of enhanced thermal pressure in the earthward motion of the Earth's magnetopause. J. Geophys. Res. 118, 3017–3026. http://dx.doi.org/10.1002/jgra50290.

Song, P., Russell, C.T., 1992. Model of the formation of the low-latitude boundary layer for strongly northward interplanetary magnetic field. J. Geophys. Res. 97 (A2), 1411–1420. http://dx.doi.org/10.1029/91JA02377.

Sonnerup, B.U.O., Paschmann, G., Papamastorakis, I., Sckopke, N., Haerendel, G., Bame, S.J., Asbridge, J.R., Gosling, J.T., Russell, C.T., 1981. Evidence for magnetic field reconnection at the Earth's magnetopause. J. Geophys. Res. 86 (A12), 10049–10067. http://dx.doi.org/10.1029/JA086iA12p10049.

Spreiter, J.R., Summers, A.L., Alksne, A.Y., 1966. Hydromagnetic flow around the magnetosphere. Planet. Space Sci. 14 (3), 223–253. http://dx.doi.org/10.1016/0032-0633(66)90124-3.

Suvorova, A.V., Shue, J.-H., Dmitriev, A.V., Sibeck, D.G., McFadden, J.P., Hasegawa, H., Ackerson, K., Jelínek, K., Šáfranková, J., Němeček, Z., 2010. Magnetopause expansions for quasi-radial interplanetary magnetic field: THEMIS and Geotail observations. J. Geophys. Res. 115, A10216. http://dx.doi.org/10.1029/2010JA015404.

Tóth, G., Sokolov, I.V., Gombosi, T.I., Chesney, D.R., Clauer, C.R., de Zeeuw, D.L., Kóta, J., 2005. Space weather modelling framework: a new tool for the space science community. J. Geophys. Res. 110, A12226. http://dx.doi.org/10.1029/2005JA011126.

Tóth, G., De Zeeuw, D.L., Gombosi, T.I., Manchester, W.B., Ridley, A.J., Sokolov, I.V., Roussev, I.I., 2007. Sun-to-thermosphere simulation of the 28–30 October 2003 storm with the Space Weather Modeling Framework. Space Weather 5, S06003. http://dx.doi.org/10.1029/2006SW000272.

Welling, D.T., Ridley, A.J., 2010. Validation of SWMF magnetic field andplasma. Space Weather 8, S03002. http://dx.doi.org/10.1029/2009SW000494.

Zhang, J., et al., 2007. Understanding storm-time ring current development through data-model comparisons of a moderate storm. J. Geophys. Res. 112, A04208. http://dx.doi.org/10.1029/2006JA011846.